Supporting Information

Orozco et al. 10.1073/pnas.1722434115

SI Materials and Methods

IHC and Immunofluorescence. For IHC, the following primary antibodies were used: anti-Gal1 (Abcam), anti-CK19 (Abcam), anti–P-HisH3 (Millipore), anti–α-SMA (Sigma), anti-vWF (Neomarkers), anti-CD31 (Spring Biosciences), anti-Ki67 (Novocastra), anti-Foxp3 (eBioscience), anti-CD3 (Santa Cruz), and anti-CD8 (Abcam). Anti-mouse or anti-rabbit HRP (Envision + reagent) was used as a secondary antibody, followed by development with 3,3′-diaminobenzidine-tetrahydrochloride (DAB) substrate (Dako). Tissues were counterstained with hematoxylin, and cover slides were assembled with DPX fixation reagent (Sigma). For immunofluorescence studies, cells were seeded over sterile coverslips in a 24-well plate, fixed with 4% paraformaldehyde, and quenched using a solution of NH_4Cl (0.1 M). Permeabilization and blocking were performed with PBS, 1% BSA, and 0.3% Triton X-100, and coverslips were incubated with anti–α-SMA (Sigma) or P-HisH3 (Millipore) antibodies, TRITC-phalloidin (Sigma), and DAPI (Sigma). Alexa-488 (Invitrogen) was used as the secondary antibody.

Flow Cytometry of Tumor-Associated Immune Infiltrates. One million cells were used for surface antibody staining and for unstained or FMO controls. Blocking of cell-surface Fc receptors was achieved with rat anti-mouse CD16/CD32 antibody. The surface-marker antibodies used were PerCP rat anti-mouse CD8; PE-Cy7 rat anti-mouse CD11b; PE rat anti-mouse Ly6G–Ly6C (Gr-1); FITC rat anti-mouse CD45; APC-Cy7 anti-mouse CD3, and BV510 rat anti-mouse CD4. All mentioned antibodies were from BD Biosciences.

Microarray Analysis and Bioinformatics. After quality control of raw data, microarray data were background-corrected, quantile-normalized, and summarized to a gene level. A moderated t-statistics model was used for detecting differentially expressed genes between the conditions. Genes with a P value < 0.01 were selected as significant and are identified in Dataset S1. Ingenuity Pathway Analysis (Ingenuity Systems, https://www.qiagenbioinformatics.com/) was used to functionally analyze the results. GO analysis was also conducted using the functional annotation tool available through the DAVID Bioinformatics Database (1, 2).

1. Dennis G, et al. (2003) DAVID: Database for annotation, visualization, and integrated discovery. *Genome Biol* 4:3.

2. Huang DW, Sherman BT, Lempicki RA (2009) Systematic and integrative analysis of large gene lists using DAVID bioinformatics resources. *Nat Protoc* 4:44–57.

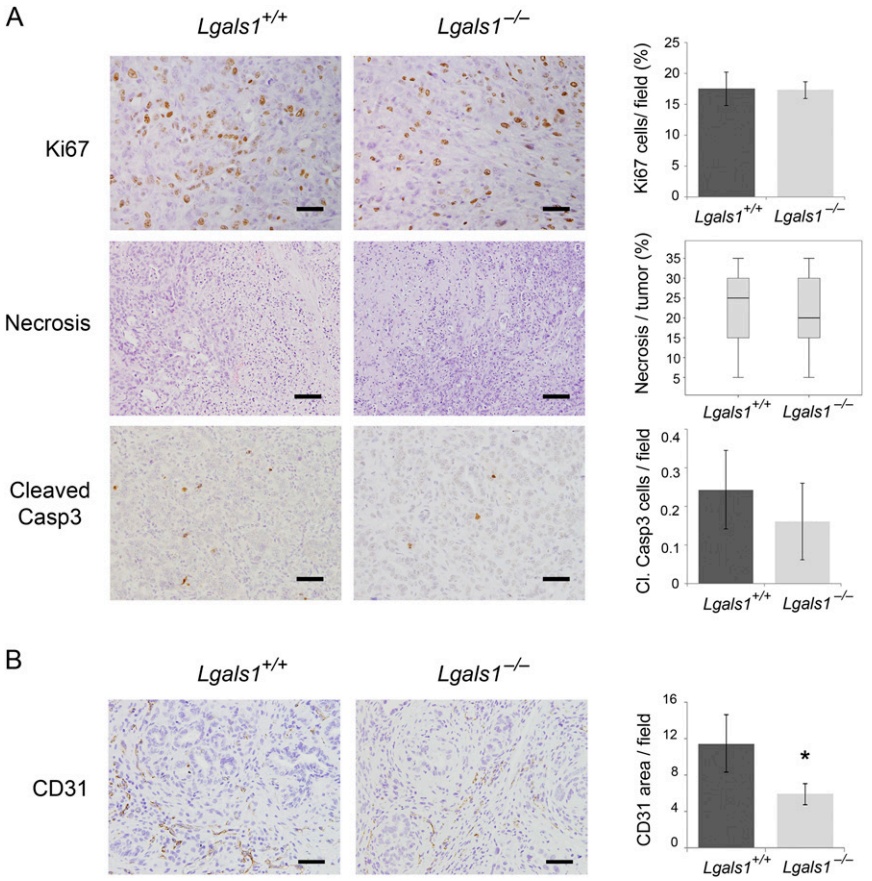

Fig. S1. Analysis of tumor proliferation, necrosis, apoptosis, and angiogenesis of pancreatic tumors from 4-mo-old *Ela-Kras*^{G12V}*p53*$^{-/-}$*Lgals1*$^{+/+}$ or *Ela-Kras*^{G12V}*p53*$^{-/-}$*Lgals1*$^{-/-}$ mice. (*A*, *Left*) Tumor cell proliferation was evaluated by Ki67 immunohistochemistry, necrosis by H&E staining, and apoptosis through immunohistochemical detection of cleaved caspase-3 (Cl. Casp3). (*Right*) Quantifications are expressed as the percentage of Ki67^{+} cells relative to the total number of cells (hematoxylin staining), the percentage of area with necrosis relative to the whole tumor area, and the number of cleaved caspase-3 cells per field. (*B*, *Left*) Tumor angiogenesis was measured by immunohistochemical analysis of CD31. (Scale bars: 50 μm.) (*Right*) Quantification expressed as the percentage of a CD31^{+} area per field. *$P < 0.05$.

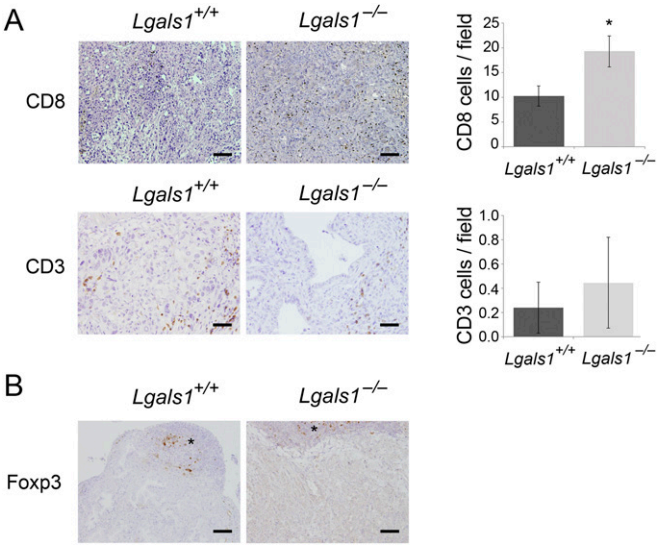

Fig. S2. Immunohistochemical detection of immune cell infiltrates. (*A*, *Left*) CD8^{+} and CD3^{+} T lymphocytes were detected by IHC in pancreatic tumor samples from 4-mo-old *Ela-Kras*^{G12V}*p53*$^{-/-}$*Lgals1*$^{+/+}$ or *Lgals1*$^{-/-}$ mice. (Scale bars: 100 μm for CD8 staining and 50 μm for CD3 staining.) (*Right*) Quantifications are expressed as the number of positive cells per field. *$P < 0.05$. (*B*) Foxp3 IHC in tumors of 4-mo-old *Ela-Kras*^{G12V}*p53*$^{-/-}$*Lgals1*$^{+/+}$ or *Lgals1*$^{-/-}$ mice. Positive cells were found in pancreatic lymph nodes (asterisks) but were not detected in pancreatic tumors from the *Ela-Kras*^{G12V}*p53*$^{-/-}$ mice. (Scale bars: 100 μm.)

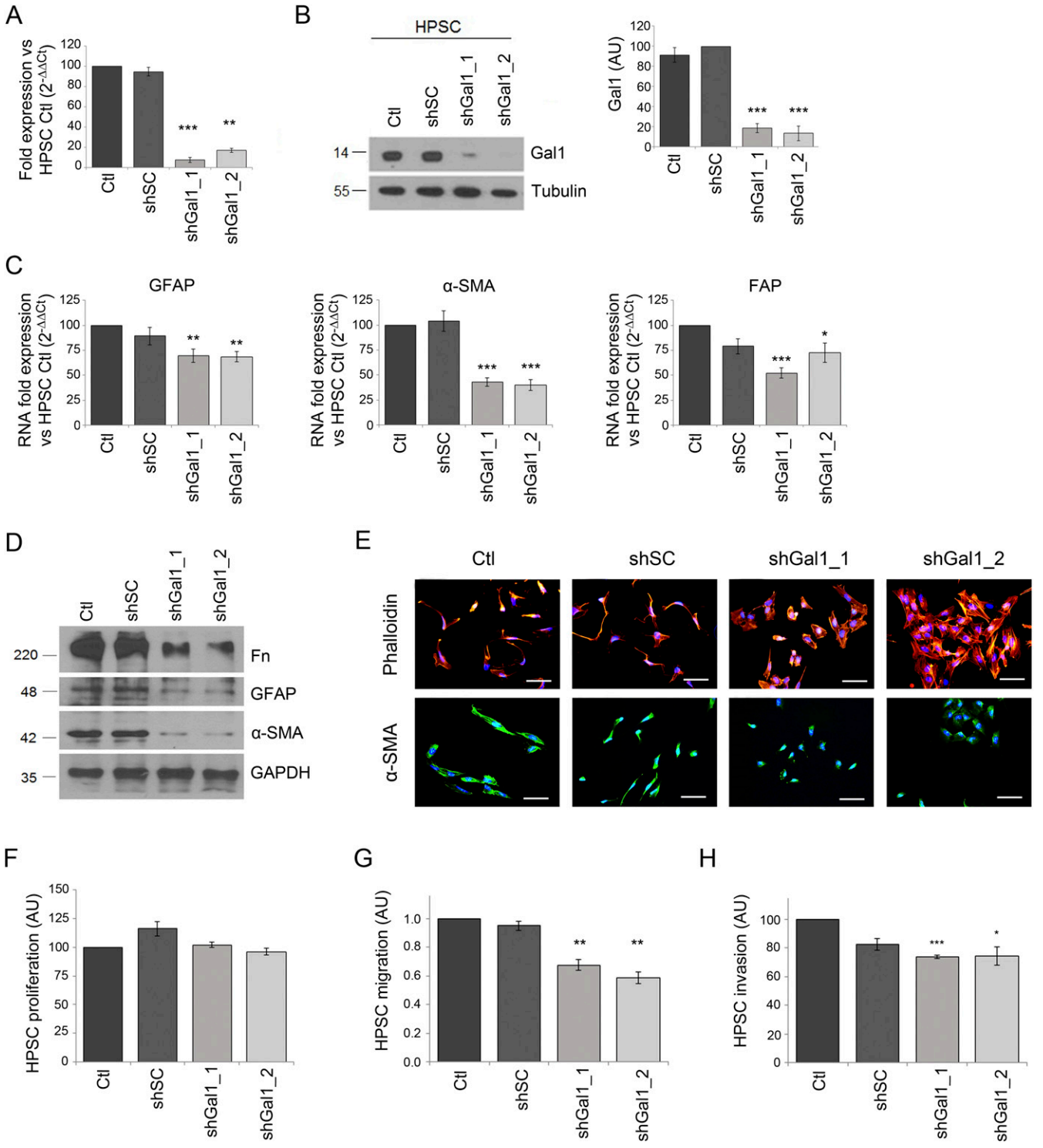

Fig. S3. Characterization and phenotypic effects of Gal1 knockdown in HPSCs. (*A*) Gal1 RNA expression levels in control HPSCs (Ctl) and in HPSCs infected with shSC or with one of two different Gal1-specific shRNA sequences (shGal1_1 and shGal1_2). (*B*) Western blot analysis (*Left*) and quantification (*Right*) of Gal1 protein expression levels in total extracts from HPSCs after shGal1 down-regulation. (*C*) RNA expression levels by RT-qPCR of fibroblast-activation markers (GFAP, α-SMA, and FAP) in control HPSCs and in HPSCs infected with shSC, shGal1_1, or shGal1_2. (*D*) Protein expression levels by Western blot analysis of fibronectin and fibroblast activation markers (GFAP and α-SMA) in HPSCs after shGal1 down-regulation. (*E*) Morphological effects of Gal1 down-regulation in HPSCs observed by immunofluorescence using antibodies against phalloidin and α-SMA. (Scale bars: 100 μm.) (*F*) Effects of Gal1 knockdown on HPSC proliferation as measured by MTT staining. (*G*) Effects of Gal1 knockdown on HPSC migration using the wound-healing assay. (*H*) Effects of Gal1 knockdown on HPSC invasion using Matrigel-coated Transwells. Data are given as the mean ± SEM of three independent experiments. $*P < 0.05$; $**P < 0.01$; $***P < 0.001$ relative to control HPSCs.

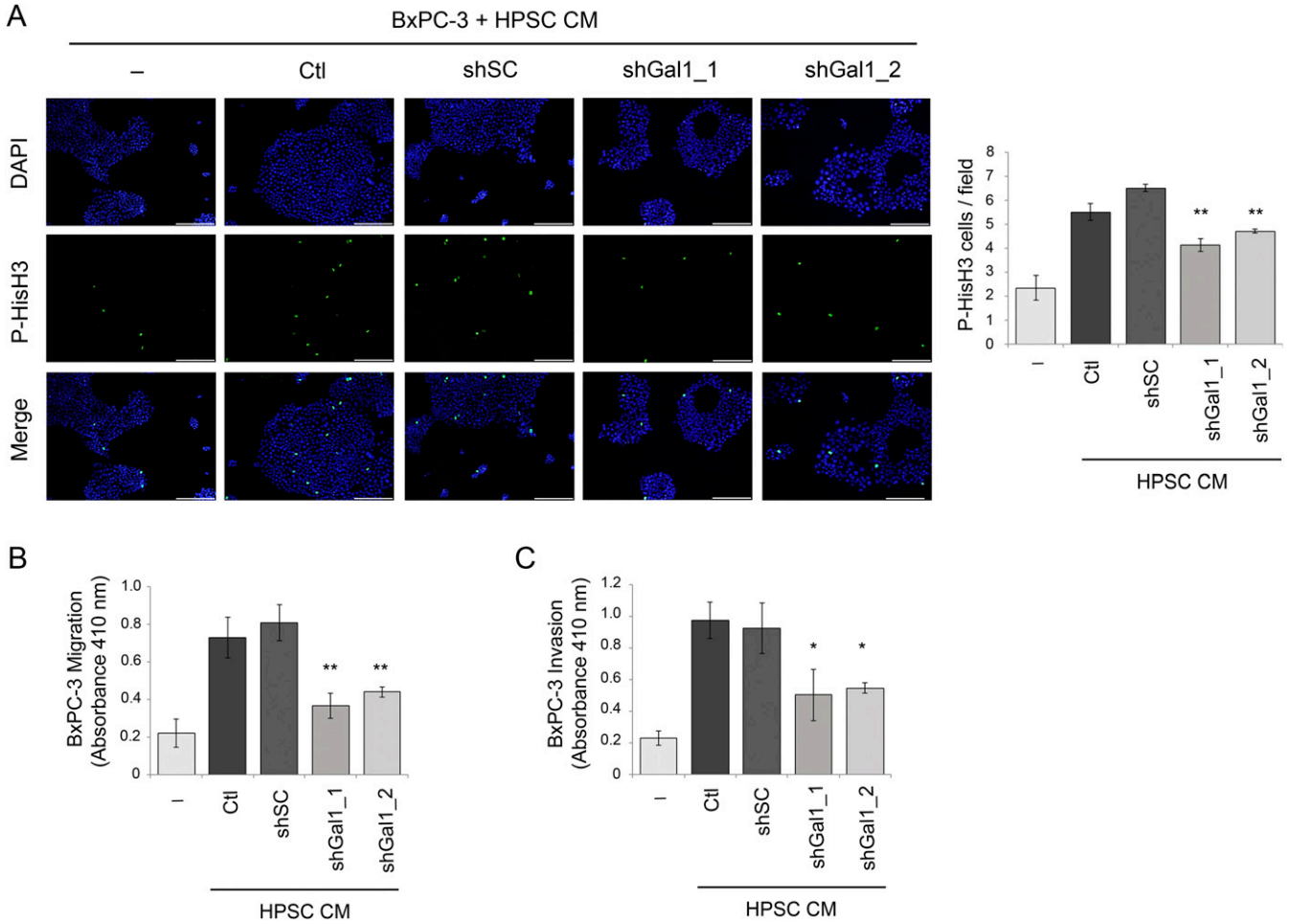

Fig. S4. HPSCs control BxPC-3 pancreatic tumor cells via Gal1. (*A*, *Left*) Effects of conditioned medium from Gal1-depleted HPSCs on BxPC-3 cell proliferation using the P-HisH3 marker. (Scale bars: 100 μm.) (*Right*) Quantification expressed as the percentage of P-HisH3^{+} cells. (*B*) Effects of conditioned medium from Gal1-depleted HPSCs on BxPC-3 cell Transwell migration as detected by hexosaminidase. (*C*) Effects of conditioned medium from Gal1-depleted HPSCs on BxPC-3 invasion analyzed by Matrigel-coated Transwell invasion experiments. Data are given as the mean ± SEM of three independent experiments. *$P < 0.05$; **$P <$ 0.01 relative to shSC.

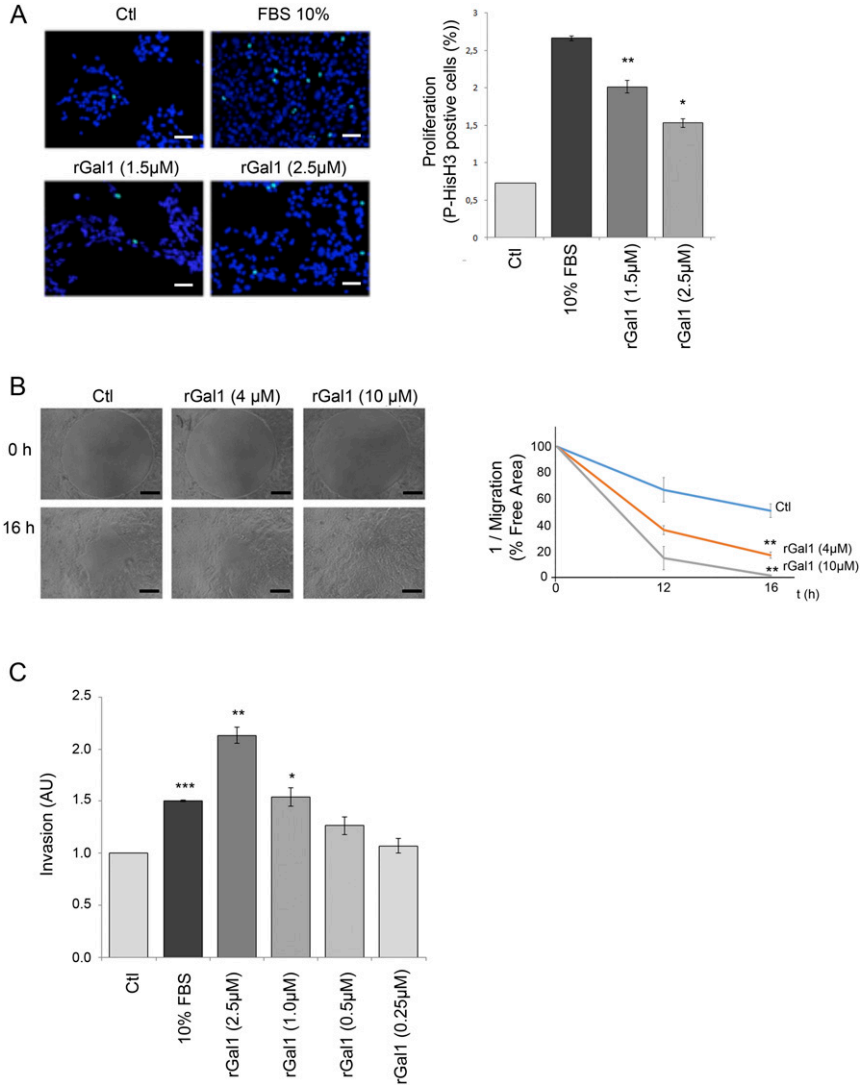

Fig. S5. Recombinant Gal1 induces proliferation, migration, and invasion of human pancreatic tumor cells. RWP-1 cells were treated with rGal1 at different doses, and functional studies were performed. (*A*) Tumor cell proliferation was measured by immunofluorescence staining with an antibody against P-HisH3. (*Left*) Representative images from the immunofluorescence staining showing P-HisH3 (green) and DAPI (blue) in untreated RWP-1 cells (Ctl) and in cells treated with 10% FBS (positive control) or with 1.5 or 2.5 μM rGal1. (Scale bars: 20 μM.) (*Right*) Quantification of the percentage of P- HisH3^{+} cells. (*B*) RWP-1 cell migration was analyzed in a gap-closure cell-migration assay. Cells growing in 2% FBS were used as negative control. (*Left*) Representative images of gap closure after 0 h or 16 h. (Scale bar: 100 μM.) (*Right*) Quantification of the migration by determining the free-area percentage at the indicated times in comparison with t = 0 h. (*C*) Tumor cell invasion was evaluated using a 96-well Transwell plate coated with Matrigel. The number of invading cells in the lower compartment was measured after 72 h using the hexosaminidase assay. Results are expressed as arbitrary units (AU) relative to values from untreated cells (0% FBS, negative control). Data are given as the mean ± SEM of three independent experiments. *$P < 0.05$; **$P < 0.01$; ***$P < 0.001$ (Student's *t* test) relative to control cells.

Table S1. Survival analysis of *Ela-Kras^{G12V}p53$^{-/-}$Lgals1$^{+/+}$* and *Lgals1$^{-/-}$* mice

Genotype	*n*	Median survival, mo	95%CI		No. surviving <3 mo (%)	No. surviving 3–6 mo (%)	No. surviving >6 mo (%)
			Lower limit	Upper limit			
Lgals1$^{+/+}$	20	3.567	3.274	3.859	4 (20.0)	14 (70.0)	2 (10.0)
Lgals1$^{-/-}$	19	4.367	2.992	5.741	1 (5.3)	11 (57.9)	7 (36.8)*

Median survival in months, 95% CI, and number of mice in each survival range are shown.
*$P < 0.05$, χ^2 test.

Table S2. Diseases and biological functions obtained from Ingenuity Pathway Analysis

Top diseases/biological functions	*P* value	No. molecules
Diseases and disorders		
Cancer	2.01^{E-03}–4.25^{E-02}	62
Organismal injury and abnormalities	2.01^{E-03}–4.25^{E-02}	7
Reproductive system disease	2.01^{E-03}–4.25^{E-02}	12
Tumor morphology	2.01^{E-03}–7.43^{E-03}	2
Connective tissue disorders	3.72^{E-03}–7.43^{E-03}	3
Molecular and cellular functions		
Cell cycle	1.74^{E-03}–4.73^{E-02}	6
Cellular movement	2.01^{E-03}–3.66^{E-02}	5
Cell morphology	3.72^{E-03}–2.94^{E-02}	3
Cellular assembly and organization	3.72^{E-03}–1.85^{E-02}	2
Cellular compromise	3.72^{E-03}–7.43^{E-03}	2

The top five disease networks and top five biological functions with the respective number of molecules within each network are shown.

Table S3. Sequences used for RT-qPCR

Gene	Forward primer (5′–3′)	Reverse primer (5′–3′)
HPRT	GGCCAGACTTTGTTGGATTTG	TGCGCTCATCTTAGGCTTTGT
GAPDH	GCGTCT CTGCTCCTCCTGTT	CCATGGTGTCTGAGCGATGT
LGALS1	CAGCAACCTGAATCTCAAACC	AAAGACAGCAACAACCTGTGC
GFAP	ATGCATGAAGCCGAAGAGTG	AGGTCAAGGACTGCAACTGG
α-SMA	TCCTCCCTTGAGAAGAGTTACG)	AGCATAGAGGTCCTTCCTGATG
FAP	TCAGCTATGATGCCATTTCG)	ATTTATGGCCTCCCACTTGC
MMP1	TGATGTGGCTCAGTTTGTCC	GCTTTCTCAATGGCATGGTC
IL1A	GGTTCTGAAGAAGAGACGGTTG	CAGGAAGCTAAAAGGTGCTGAC
ASXL3	CACCAATGACAGCAAAGCAG	TGTTCCATCCCCTATTCGAG
EXTL2	AATCGACTCCAGGTCTTTCC	GAAAGCAAAAACAAGGTCTGG
AGAPAT9	GTCATAGTGCGCTATTGTGTCC	CCAGCAAACTGATCCCAATG
GALNT16	GCCATGTCTTCAGGAAACG	TCATCCATCCACACTTCTGC
GPCD1	TGGATTCTGGATGGCTGAC	TTCCTCCAGGCCTTCTAGTG
ANK3	TCAAGCATCTTTCCCAGAGG	TTCCGTCTTCTTGGTTCCAC
TOX	TGGCCTGCTACCATTTCATC	TGAGTTCCTTCTGGGTTTCG
DHCR7	GACAACTGGATCCCACTGCT	TCCGAGGGTTAAACTCGATG
TFRC	TGTGAGCAATGTGCTGAAAG	AGGAGAGCTGTGCCTACACC
INSIG1	GTGATCGCCACCATCTTTTC	TGACACTGGCCCATTCTCTC
CLCNK8	AGTGGCTGAAGCAGAAGCTC	CAGGAGAGATACCGGAGCAG
ROCK1	GCAAAGTCTGTGGCAATGTG	CGATTTTCAGCCTTCTCTCG

Other Supporting Information Files

Dataset S1 (XLS)